Environmental Science & Technology

Article

pubs.acs.org/est

Visible Light Assisted Heterogeneous Fenton-Like Degradation of Organic Pollutant via α-FeOOH/Mesoporous Carbon Composites

Xufang Qian, Meng Ren, Yao Zhu, Dongting Yue, Yu Han, Jinping Jia, and Yixin Zhao*

School of Environmental Science and Engineering, Shanghai Jiao Tong University, 800 Dongchuan Rd., Shanghai 200240, China

Supporting Information

ABSTRACT: A novel α-FeOOH/mesoporous carbon (α-FeOOH/MesoC) composite prepared by in situ crystallization of adsorbed ferric ions within carboxyl functionalized mesoporous carbon was developed as a novel visible light assisted heterogeneous Fenton-like catalyst. The visible light active α-FeOOH nanocrystals were encapsulated in the mesoporous frameworks accompanying with surface attached large α-FeOOH microcrystals via C−O−Fe bonding. Assisting with visible light irradiation on α-FeOOH/MesoC, the mineralization efficiency increased owing to the photocatalytic promoted catalyzing H_2O_2 beyond the photothermal effect. The synergistic effect between α-FeOOH and MesoC in α-FeOOH/MesoC composite improved the mineralization efficiency than the mixture catalyst of α-FeOOH and MesoC. The iron leaching is greatly suppressed on the α-FeOOH/MesoC composite. Interestingly, the reused α-FeOOH/MesoC composites showed much higher phenol oxidation and mineralization efficiencies than the fresh catalyst and homogeneous Fenton system ($FeSO_4/H_2O_2$). The XPS, XRD, FTIR, and textural property results reveal that the great enhancement comes from the interfacial emerged oxygen containing groups between α-FeOOH and MesoC after the first heterogeneous Fenton-like reaction. In summary, visible light induced photocatalysis assisted heterogeneous Fenton-like process in the α-FeOOH/MesoC composite system improved the HO• production efficiency and Fe(III)/Fe(II) cycle and further activated the interfacial catalytic sites, which finally realize an extraordinary higher degradation and mineralization efficiency.

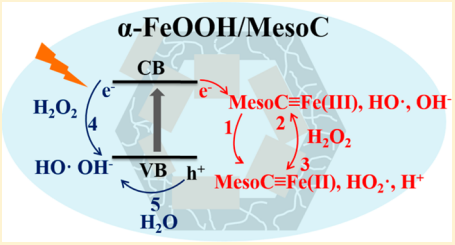

INTRODUCTION

Fenton reaction is an effective method for degradation of stubborn organic pollution; however, the classical Fenton reaction has two obvious shortcomings: the low activities at neutral or basic condition; the significant iron residue related second pollution. To overcome these shortcomings, the various Fenton-like reactions have been developed. The heterogeneous Fenton-like reaction at neutral condition has been widely studied. The key for heterogeneous Fenton-like reaction is developing an efficient heterogeneous Fenton-like catalysts to overcome the challenge of iron leaching and low catalytic activity.[1−3] Inert porous materials such as zeolites, clay, metal oxides, mesoporous silica, porous carbon, sp^2 type graphite (graphene, graphene oxide, carbon nanotubes) with large surface area were commonly used as supports for increasing the dispersion of active sites and preventing metal ion leaching.[4−9] These carbon-based materials used in advanced oxidation process have the advantages of high chemical and thermal stability, high surface area with controllable surface chemistry and easy metal recovery.[10] Among them, the commercial activated carbon (AC) has been widely used in large scale application. However, AC usually contains metal or nonmetal impurities and its surface chemistry is difficult to control, which make it difficult for fundamental investigation of the AC based composite catalysts.[10−14] On the other hand, the activation of H_2O_2 by metal free carbon based materials is highly correlated to their unique surface chemistry such as basic active sites, acidic oxygen containing groups, reductive sites etc.[10,15] Therefore, it is promising to improve and/or assist the heterogeneous Fenton reaction by modifying the surface chemistry of carbon materials. Ordered mesoporous carbon prepared by self-assembly has the advantages of ordered mesostructure and the tunable textural/surface properties are promising for heterogeneous catalysis with better adsorption/separation performance.[16−18] Goethite (α-FeOOH) is a natural mineral ubiquitous in soils, sediments at the earth surface. Owing to its abundance and availability, relative stability and low cost, goethite has been widely used in environmental scavenger and water treatment.[19] However, the ineffective Fe(III)/Fe(II) cycle in goethite limits their efficiency for Fenton reaction to decompose stubborn organic pollutants.[20] Up to now, many efforts such as addition of ascorbic acid have been made to enhance the Fe(III)/Fe(II) cycle on the surface of $Fe@Fe_2O_3$ and in the solution.[21] UV and ultrasonic irradiation were also developed to improve the Fe(III)/Fe(II) cycle in the heterogeneous Fenton-like reaction.[22−25]

In order to efficient utilization of solar energy to assist the heterogeneous Fenton-like reaction for advanced oxidation process, a visible light assisted heterogeneous Fenton-like catalysts system is highly desired.[26−28] Here, we develop an effective low toxic iron based heterogeneous Fenton-like

Received: December 20, 2016
Revised: March 3, 2017
Accepted: March 3, 2017
Published: March 3, 2017

DOI: 10.1021/acs.est.6b06429
Environ. Sci. Technol. 2017, 51, 3993−4000

Scheme 1. Illustrative Procedure for Synthesis of the α-FeOOH/MesoC Composite

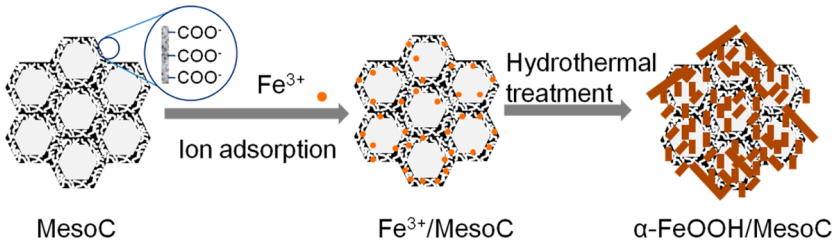

catalysts by combining the traditional α-FeOOH with ordered mesoporous carbon to decomposition of stubborn organic pollutant of phenol.[25,29,30] With the visible light irradiation, the mineralization efficiency of phenol increased by 40% after 2 h reaction at pH 5 in comparison with the case in dark. The composite catalyst showed obvious superiority relative to the mixture owing to the interaction between α-FeOOH and MesoC. Iron leaching was largely suppressed for the composite catalyst. The activity was greatly increased for the reused α-FeOOH/MesoC composite and the intrinsic property change after reaction was investigated. A schematic illustration of photocatalysis promoted heterogeneous Fenton process under visible light irradiation on the α-FeOOH/MesoC composite was proposed.

EXPERIMENTAL SECTION

Chemicals and Reagents. Poly(propylene oxide)-*block*-poly(ethylene oxide)-*block*-poly(propylene oxide) triblock copolymer Pluronic F127($PEO_{106}PPO_{70}PEO_{106}$, Mw = 12 600) was purchased from Sigma−Aldrich. Sodium hydroxide (NaOH, ≥ 96%), hydrochloric acid (HCl,36.0−38.0 wt %), hydrogen peroxide (H_2O_2, 30%), hydrofluoric acid (HF, ≥ 40%), formalin solution (HCHO, 37.0−40.0 wt %)were obtained from Shanghai Lingfeng Chemical Reagent Co., Ltd. Phenol (C_6H_5OH, ≥ 99.0 wt %), ethanol (C_2H_5OH, ≥ 99.7 wt %), iron(III) nitrate nonahydrate ($Fe(NO_3)_3{\cdot}9H_2O$, ≥ 98.5 wt %), ammonium persulfate ($(NH_4)_2S_2O_8$, ≥ 98.5 wt %), sulfuric acid (H_2SO_4, 95−98 wt %) were obtained from Sinopharm Chemical Reagent Co., Ltd. Titanium sulfate ($TiOSO_4$) was purchased from Aladdin Industrial Corporation. 5,5-dimethyl-pyrroline-1-oxide (DMPO) was obtained from Tokyo Chemical Industry Co., Ltd. All the aqueous solutions were prepared by using distilled and deionized water.

Catalysts Preparation. The ordered mesoporous carbon was prepared according to the literature method.[31] The obtained ordered mesoporous carbon was treated by a wet oxidation method to make it hydrophilic.[32] The iron species were introduced by an adsorption process. Typically, 0.1 g of hydrophilic ordered mesoporous carbon were immersed in 25 mL of 0.14 M $Fe(NO_3)_3{\cdot}9H_2O$ solution with stirring for 12 h. After the above adsorption process, the product were washed with distilled water and then transferred into a 100 mL of beaker with 5 mL distilled water in it. Subsequently, 9 mL of 5 M NaOH were added rapidly with stirring for 30 s and the suspension was immediately diluted to 100 mL with distilled water. Then the mixture was transferred into a 150 mL Telfon-lined autoclave, followed by the hydrothermal reaction at 70 °C for 12 h. Finally, the obtained precipitates were washed and dried in vacuum at 40 °C, named as α-FeOOH/MesoC.

Characterization. X-ray diffraction (XRD) patterns were measured on a Shimadzu XRD-6100 diffractometer using Cu Kα as radiation. Field-emission scanning electron microscopy (FESEM) was obtained on a JSM-7800F Prime scanning electron microscope. Transmission electron microscopy (TEM) images were performed on a JEOL-JEM-2010 microscope. Nitrogen sorption isotherms were measured at 77K with a Micromeritics Tristar 3000 analyzer. Before measurements, the samples were degassed in a vacuum at 70 °C for at least 6 h. Fourier transform infrared (FT-IR) spectra were obtained on a Tensor 27 FTIR spectrometer (Nicolet 6700), using KBr pellets of the blank. The iron content of the composite catalysts was measured by inductively coupled plasma-optical emission spectrometry (iCAP 6000 Radial). The chemical state analysis of iron for composite catalysts was investigated by X-ray photoelectron spectroscopy (XPS, AXIS ULTRA DLD). Electron paramagnetic resonance (EPR) from a Bruker EMX-8/2.7C was applied to probe the reactive radicals generated during activation of H_2O_2 captured by a spin trapping agent 5,5-dimethylpyrroline-oxide (DMPO), operating with center field at 3515G, sweep width of 200G, microwave frequency of 9.88 GHz, power setting of 6.39 mW, and scan number of 1.

Procedures and Analysis. Heterogeneous Fenton-like oxidation of phenol was performed in dark and visible light irradiation for evaluating the catalytic activity of composite catalysts. Typically, 10 mg of catalyst and 20 mL of 100 mg/L phenol was added into the self-made quartz flask and stirred for 30 min to achieve adsorption/desorption equilibrium of phenol. Next, the pH was adjusted to a targeted value by using 0.1 M H_2SO_4 or 0.1 M NaOH. After that, 60 μL H_2O_2 was added and the flask was sealed immediately by a rubber plug and parafilm. Gas samples were collected from the top of the flask using a 500 μL syringe at different time intervals and then injected into a gas chromatography (GC7900) to detect CO_2 for calculating the mineralization efficiency of phenol. Then the flask was placed in front of a 100W white LED lamp (CEL-LED100) (Supporting Information (SI) Figure S1) with a 420 nm cut filter. Before the lamp was switched on, it took 10 min for H_2O_2 diffusion. According to the stoichiometric consumption of $[H_2O_2]$ calculated based on eq 1,

$$C_6H_6O + 14H_2O_2 \rightarrow 6CO_2 + 17H_2O \quad (1)$$

the mineralization efficiency was calculated by the following equation,

$$\text{mineralization efficiency} = \frac{[CO_2]}{6 \times [\text{phenol}]} \times 100\% \quad (2)$$

In addition to measuring the mineralization efficiency, the stability of α-FeOOH/MesoC was tested by recovering the solid catalyst via filtration and drying. At a given interval, 1 mL aliquots were collected and filtered through a Millipore filter for Waters 1515 gel permeation chromatography (GPC) analysis of phenol degradation. Water and methanol (80:20, v/v) were mixed as the mobile phases. The H_2O_2 concentration was analyzed colorimetrically on the UV spectrophotometer (Cary

DOI: 10.1021/acs.est.6b06429
Environ. Sci. Technol. 2017, 51, 3993−4000

60 UV−vis) after complexation with a $TiOSO_4/H_2SO_4$ reagent.[33] The wavelength was set at 410 nm. The iron leaching during reaction was analyzed using spectrophotometrically at 510 nm using phenanthroline method.

RESULTS AND DISCUSSION

The α-FeOOH/MesoC composite was synthesized by in situ hydrothermal treatment of Fe^{3+}/mesoporous carbon in basic media as shown in Scheme 1. The crystallinity was controlled by changing the hydrothermal time. The electrostatic interaction of Fe^{3+} and mesoporous carbon with plenty of carboxyl groups induces the confining of iron species within the mesoporous frameworks (SI Figure S2).

The XRD pattern of α-FeOOH was shown in Figure 1a, the diffraction peaks of the α-FeOOH/MesoC composite are consistent with typical goethite crystalline phase (JCPDS file: 00−029−713) without any impurity peaks. The α-FeOOH/MesoC composites show the goethite crystals grown on MesoC surface are the typical acicular (100−300 nm along *b* direction) and elongated (1−3 μm) along the crystallographic *c* direction (Figure 1b). The twining of goethite crystals is observed for the α-FeOOH/MesoC composite similar to the pure α-FeOOH.

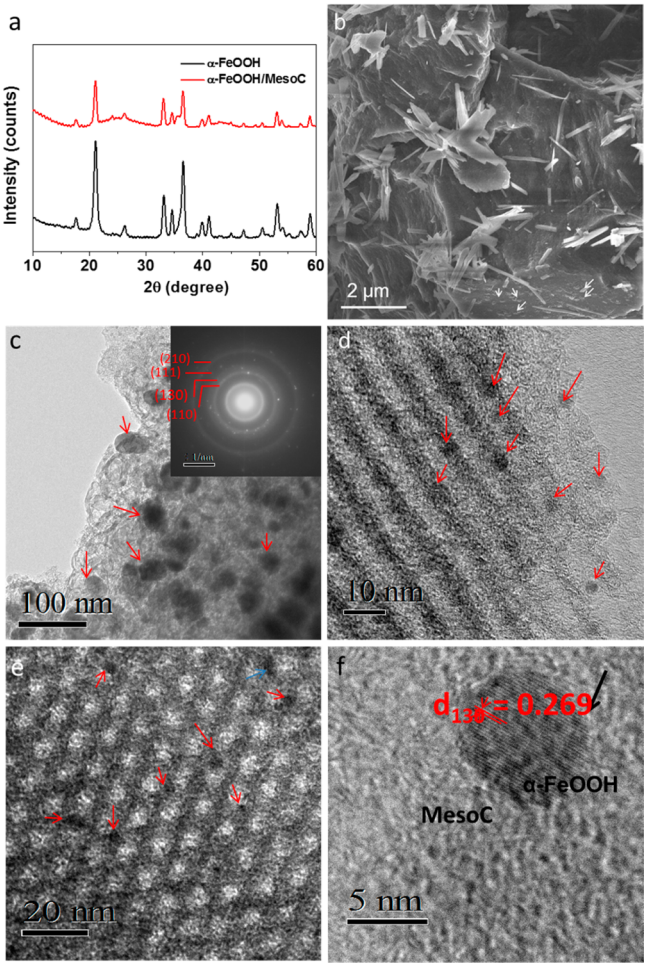

Figure 1. Wide-angle XRD patterns of pure α-FeOOH and the α-FeOOH/MesoC composites (a), SEM and TEM images of α-FeOOH/MesoC composite (b−f). The white arrows in b denote a large amount of α-FeOOH nanocrystals. The SAED was shown in inset of c. The red arrows in c−e denote the α-FeOOH nanocrystals.

Figure 1b shows some small α-FeOOH nanocrystal cubes with average crystal size of 80 nm dispersed on the surface of MesoC in α-FeOOH/MesoC. As shown in Figure 1c, nanoparticles with sizes around 80 nm are dispersed on the mesoporous carbon which is in agreement with the small α-FeOOH nanocrystal cubes observed on SEM image. The corresponding selected area electron diffraction (SAED) pattern shows that the diffraction spots are superimposed on the rings assigning to planes (110), (130), (111), and (210) of α-FeOOH nanocrystal indicating the polycrystalline nature, whereas the ∼5 nm nanoparticles are encapsulated within mesopores (Figure 1de). HRTEM image of a nanoparticle shows lattice fringe spacing of 0.269 nm, which can be assigned to the plane (130) of α-FeOOH (Figure 1f). The above results indicate the confining of α-FeOOH nanocrystals in the MesoC frameworks. The obtained α-FeOOH/MesoC composites are deep brown color without visual observation of yellow color indicating the uniform dispersion of α-FeOOH on MesoC (as shown in SI Figure S3a−c). The UV−vis spectrum of pure α-FeOOH shows a broad fundamental absorption band in the full spectrum of 200−800 nm (SI Figure S 3d). Owing to the dark color of α-FeOOH/MesoC composite, the corresponding UV−vis absorption band is difficult to reflect the intrinsic nature of supported α-FeOOH.

The BET results in SI Figure S4 suggest that the pore size of the α-FeOOH/MesoC composite is around 6 nm with a narrow distribution. The above results indicate the MesoC support retained the ordered mesoporous structure after immobilization of α-FeOOH treated at 70 °C. The texture properties are listed in SI Table S1. It is obviously that the specific BET surface area and total pore volume of the composite largely decreased to 47 m^2/g and 0.04 cm^3/g, respectively, which is much smaller than pure MesoC supports (S_{BET} 391 m^2/g, V_t 0.2 cm^3/g) (SI Table S1 and FigureS4). It reflects that α-FeOOH nanocrystals occupied the voids of mesopores in agreement with the TEM results.

Heterogeneous Fenton-like reaction in dark and under visible light irradiation was evaluated by using phenol as a model organic pollutant. Low operation pH value (around 3) hindered the application of homogeneous Fenton process owing to the precipitation problem of iron ions in basic condition. The pH 5 condition is usually adopted as a model condition for heterogeneous Fenton reaction evaluation. As shown in Figure 2a, the α-FeOOH/MesoC reached about 10% mineralization efficiency after 2h in dark with condition of 30 mM H_2O_2, 0.5 g/L catalyst and pH 5 at 45 °C. Upon visible light irradiation, the mineralization efficiency then increased to 14%. In order to further investigate the catalytic activity, the phenol oxidation by the α-FeOOH/MesoC composite in dark and under visible light irradiation was evaluated. The adsorption reaches equilibrium after 60 min. The phenol oxidation efficiency is 43% under visible light and 21% in dark condition, respectively. The above results clearly show that visible irradiation enhances the mineralization and oxidation activity of α-FeOOH/MesoC composite. The concentration of H_2O_2, catalyst dosage and pH values were studied on the heterogeneous Fenton-like mineralization of phenol using α-FeOOH/MesoC as a catalyst under visible light irradiation (Figure 2b−d). The mineralization efficiency improves with increasing the H_2O_2 concentration from 10 mM to 30 mM (Figure 2b). The same phenomenon is found for the effect of H_2O_2 dosage in dark condition, wherein the mineralization efficiency improves with increasing the H_2O_2 concentration from 10 mM to 30 mM (SI

DOI: 10.1021/acs.est.6b06429
Environ. Sci. Technol. 2017, 51, 3993−4000

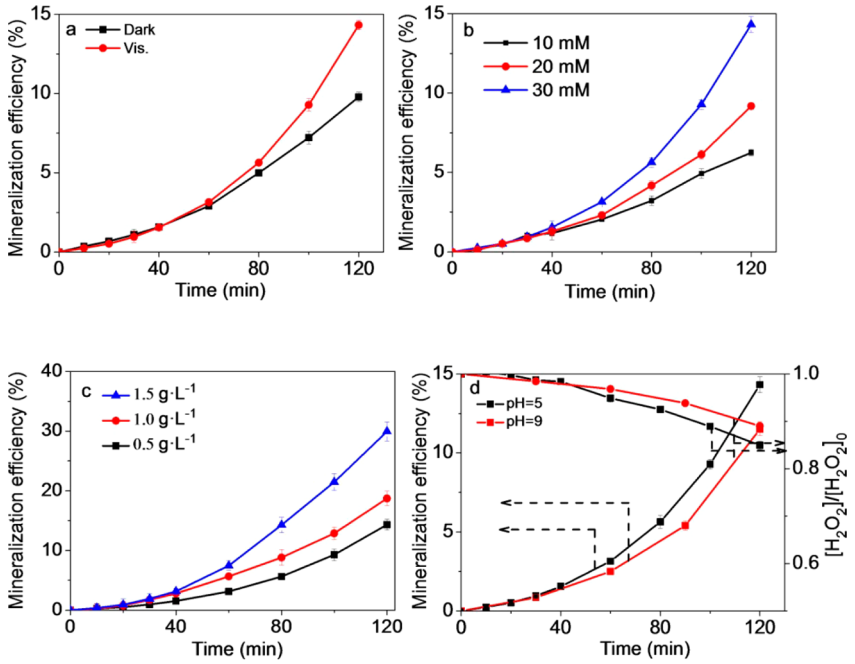

Figure 2. Mineralization efficiency of phenol on the α-FeOOH/MesoC in dark and under visible light irradiation, respectively (a); Effects of H_2O_2 dosage, catalysts concentration and pH value on phenol mineralization and the H_2O_2 consumption ratio in the α-FeOOH/MesoC suspension (b–d). Experimental conditions: 100 mg/L phenol, 0.5 g/L catalyst, initial pH of 5, 30 mM H_2O_2 and 45 °C.

Figure S6). By increasing the catalyst dosage from 0.5 g/L to 1.5 g/L, the mineralization efficiency increases from 14%, 19% to 30%, respectively, within 2 h (Figure 2c). As shown in Figure 2d, the mineralization efficiency reaches to 12% at initial pH of 9 after 2 h under visible irradiation, which is comparable to the value at pH 5 (14%). The time profiles of actual consumption ratio of H_2O_2 show that about 15% and 11% H_2O_2 was decomposed within 2 h at initial pH value of 5 and 9 respectively. The increase tendency of mineralization efficiency and consumption ratio of H_2O_2 is in good consistent indicating the predominant oxidation potential from heterogeneous Fenton-like catalysis of H_2O_2.

The durability and stability is an important aspect for evaluating a heterogeneous Fenton catalyst. Figure 3 shows the reusability of α-FeOOH/MesoC composite with successive three tests. In addition to measuring the mineralization efficiency, phenol oxidation ratio was also analyzed during 2 h reaction. In first run, phenol removal ratio reaches 52% accompanying by 14% of mineralization efficiency. It is interesting that the removal ratio reaches nearly 100% with a mineralization efficiency of 50% and 72% for second and third run, respectively. The mineralization efficiency of $FeSO_4$ homogeneous Fenton reaches 44%, which is lower than the reused α-FeOOH/MesoC composites (SI Figure S7). The above results indicate that the activity of fresh α-FeOOH/MesoC greatly improved after heterogeneous Fenton-like oxidation.

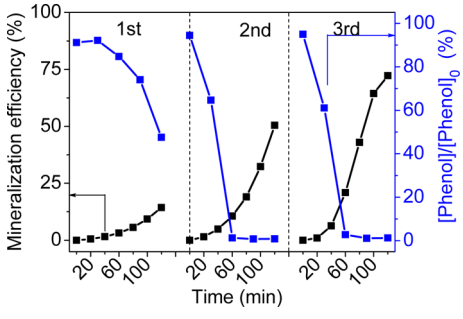

Figure 3. Reusability of Fenton-like mineralization (black) and oxidation (blue) efficiency of phenol under visible light irradiation. Experimental conditions: 20 mg/L phenol, 0.5 g/L catalyst, initial pH 5, $[H_2O_2]$ = 30 mM.

The phenol oxidation and mineralization efficiency greatly improved for the reused composite catalysts. Accordingly, XPS was used to explore the electronic structures and the interactions between the MesoC supports and α-FeOOH in the fresh and reused α-FeOOH/MesoC composites. The wide spectrum of photoelectron peaks in Figure 4a,b show the presence of C 1s, O 1s and Fe 2p. The high resolution XPS spectrum of Fe 2p core-level shows two photoelectron peaks at 711.7 eV (Fe 2p 3/2) along with a satellite peak at 719.9 and 725.3 eV (Fe 2p 1/2) together with a shakeup satellite at 733.6 eV (insets in Figure 4a,b), consisting with literature report of FeOOH.[34] High resolution O 1s peaks of the fresh and reused α-FeOOH/MesoC composites are shown in Figure 4c and d, respectively. The deconvolution of O 1s peaks of the composites includes five different peaks assigning to the oxygen in carboxyl (534.3–535.4 eV), hydroxyl, ether, carbonyl (533.1–533.8 eV), Fe–O–H (531.8 eV), Fe–O–C(531.2 eV), and Fe–O–Fe (529.8 eV), respectively.[35] The relative content of O atoms in surface Fe–O–H of the fresh α-FeOOH/MesoC is 30.0%. It should be mentioned that the relative content of O atoms in C–O–Fe for the fresh α-FeOOH/MesoC is around 30.3% indicating the interaction between α-FeOOH and MesoC support. The formation of C–O–Fe between coal and α-FeOOH had been reported in the heat treatment of $Fe(NO_3)_3$-impregnated coal with H_2O in coal gasification reaction.[36,37] The deconvolution of C 1s peaks of the composite includes five different peaks assigning to the C=C sp2 (284.6 eV), C–C sp3 (285.1 eV), C–OH and/or C–

DOI: 10.1021/acs.est.6b06429
Environ. Sci. Technol. 2017, 51, 3993–4000

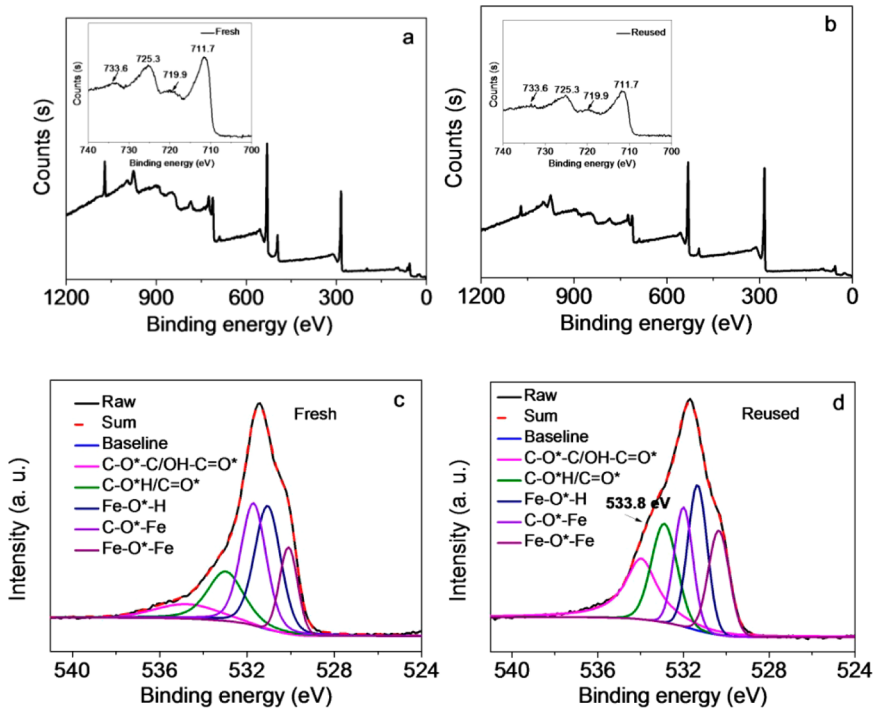

Figure 4. Wide scan XPS spectra (a, b) and high resolution XPS curve fits of O 1s (c, d) for the fresh and reused α-FeOOH/MesoC composites, respectively. Insets in Figure a,b show the high resolution XPS spectra of Fe 2p of the fresh and reused α-FeOOH/MesoC composites, respectively.

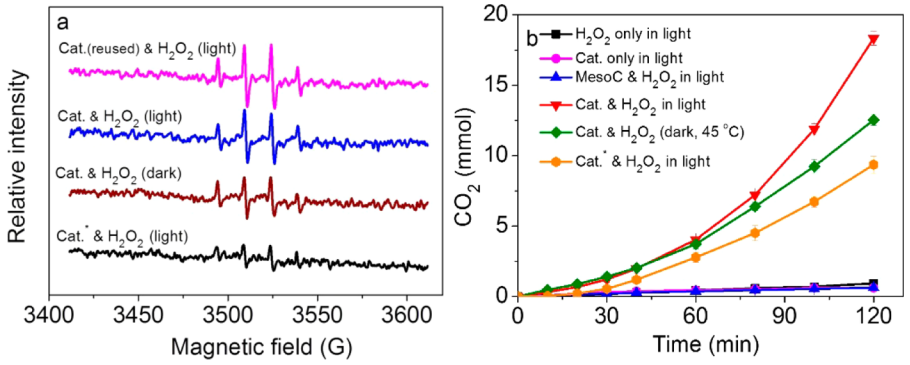

Figure 5. EPR spectral changes of the DMPO−OH adduct under various conditions (a): Cat. denotes the α-FeOOH/MesoC; Cat.* denotes the mixture of α-FeOOH and MesoC; reaction time 30 s, initial pH value of 5. Time profiles of mineralization efficiency at initial pH of 5under different conditions (b): 100 mg/L phenol, 0.5 g/L catalyst, 30 mM H_2O_2 and 45 °C.

O−C(286.7 eV), C═O (288.1 eV), and O−C═O (289.0 eV) suggesting the presence of various carbon groups (SI Figure S8).[38] The above results imply the fresh α-FeOOH/MesoC possesses plentiful surface Fe−O−H and the strong interaction between carbon support and α-FeOOH via C−O−Fe attributing to the in situ transformations process of Fe^{3+}/MesoC to α-FeOOH/MesoC composites upon hydrothermal treatment. In comparison with fresh α-FeOOH/MesoC, the high-resolution O 1s spectrum shows an obvious shoulder around 533.0 eV for reused α-FeOOH/MesoC (Figure 4d), which corresponds to the oxygen atoms in carboxylic (534.3−535.4 eV) and hydroxyl, ether, carbonyl (533.1−533.8 eV). All these results reveal that the relative contents of O atoms from oxygen functional groups of carbon surface increase obviously after heterogeneous Fenton-like reaction under visible light irradiation, which should be related to the interfacial activation, that is, carbon surface oxidation during the phenol degradation reaction.

In order to further reveal the property variation of the reused α-FeOOH, the reused α-FeOOH/MesoC was characterized by XRD, N_2 sorption and FT-IR. No obvious change and impurities is present on XRD pattern (SI Figure S9) and Fe 2p XPS spectrum of the reused α-FeOOH/MesoC indicating the unchanged component of α-FeOOH (Figure 4a, b). The S_{BET} and V_t of the reused α-FeOOH/MesoC almost keep as same as the fresh catalyst except for the slight decrease of pore size from 6.0 to 5.7 nm owing to the emerging of oxygen containing groups after reaction (SI Table S1).[32] FT-IR spectra of the reused α-FeOOH/MesoC composite show the peaks around 1930 cm^{-1}, 1720 cm^{-1}, 1574 cm^{-1}, and 1411−1026 cm^{-1} assigning to the stretching vibration of C═O, C═C, and C−O bonds, respectively (SI Figure S10), become much obvious relative to the fresh one. Calculated from XPS result, the surface oxygen concentration of fresh α-FeOOH/MesoC is 29.0% and it increases to 31.2% in the reused α-FeOOH/MesoC. These results are well consistent with the result of high

DOI: 10.1021/acs.est.6b06429
Environ. Sci. Technol. 2017, 51, 3993−4000

resolution O 1s XPS and confirm the emerging of oxygen containing groups after reaction. ESR spectrum of the reused α-FeOOH/MesoC possesses the stronger DMPO−OH adduct signals than the fresh catalyst indicating the promotion effect originating from the efficient hydroxyl radical production (Figure 5a). Recently, metal free carbon nanomaterials have been found the ability for activating H_2O_2.[25,39−43] For the reused α-FeOOH/MesoC, MesoC surface with plenty of oxygen containing groups may act as the electron-transfer mediator. On the other hand, surface oxygen groups with reducibility also can promote the cycle of ≡Fe(III)/≡Fe(II).[21]

In order to elucidate the synergistic effect, phenol mineralization efficiencies were evaluated at different conditions. The phenol adsorption capabilities of pure α-FeOOH and the fresh α-FeOOH/MesoC composite are very limited; only less than 7% phenol was removed indicating the negligible effect from pollution accumulation (SI Figure S11). As shown in Figure 5b, phenol can hardly be mineralized without catalysts or with H_2O_2 under visible light irradiation. The phenomenon indicates the visible light irradiation is unable to dissociate the H_2O_2 to produce sufficient HO• and the photocatalytic mineralization of phenol in the absence of H_2O_2 for α-FeOOH/MesoC is difficult to realize. The photocatalytic mineralization efficiency of pure α-FeOOH can be ignored (SI Figure S12). Additionally, pure MesoC is inactive in the presence of H_2O_2 and visible light. Upon visible light irradiation, the solution temperature increased from 30 to 45 °C within initial 30 min and kept unchanged (SI Figure S13). Generally, the heterogeneous Fenton activity also was influenced by the temperature. In order to exclude the temperature effect, all of the reaction was performed at 45 °C in dark. The mineralization efficiency reaches about 10% for α-FeOOH/MesoC at 45 °C in dark, which is lower than that under visible light irradiation. It implies that visible light could enhance the catalytic production of active radicals for oxidation of phenol beyond thermal effect. It should be mentioned that the mineralization efficiency of the mechanical mixture reaches only 7%, which is half of the fresh α-FeOOH/MesoC. The result means the presence of synergistic effects between α-FeOOH and MesoC account for the high activity. As Figure 5a shown, the DMPO spin-trapping ESR spectra in dark or visible light condition at same time interval appear four typical DMPO−OH adducts with intensity of 1:2:2:1 in all of the catalyst-H_2O_2 system. Upon visible light irradiation, the fresh α-FeOOH/MesoC composite shows much higher intensity of DMPO−OH adduct signal than the case of mixture containing α-FeOOH (iron of 4.7 wt %) and MesoC, whereas DMPO−OH adduct signals were stronger under visible light irradiation than that in dark. The ESR results are in good consistent with the mineralization efficiency indicating that the generated HO• through heterogeneous Fenton-like reaction resulted the phenol degradation.

Additionally, iron leaching problem during the heterogeneous Fenton reaction is concerned greatly for practical application.[1] The concentration of soluble iron ion of the filtrate after 2 h reaction at pH of 5 in visible light irradiation is 0.2 mg/L. Iron ion concentrations at pH value of 5 are much lower than the legal limit of the European Union (2.0 mg/L). The soluble iron ion concentration is 1.2 mg/L in visible light for the mixture catalyst of α-FeOOH and MesoC after 2 h reaction much higher than the composite case indicating the heterogeneous Fenton reaction rather than the homogeneous process. The composite catalyst is much stable for iron leaching than mixture due to the strong interaction of α-FeOOH and MesoC.

The mesoporous carbon in our novel heterogeneous Fenton catalyst of α-FeOOH/MesoC is very responsible for the high activity, stability and low iron leaching in degradation of phenol in the presence of H_2O_2. In comparison with other carbon based supports including activated carbon, carbon aerosol, CNTs and graphene, mesoporous carbon material with high porosity and ordered mesopore structures is very attractive for uniformly supporting and encapsulating α-FeOOH crystals to form a compact composite Fenton catalyst with sufficient interface between carbon and α-FeOOH. The porosity of the composite catalyst keeps unchanged after Fenton reaction further reflecting the stable composite structure. Mesoporous carbon derived from phenolic resin contains a certain number of organic groups with C, H elements which can be oxidized at the interface of composite catalysts during Fenton reaction,[44] these oxidized groups may act as catalytic sites for H_2O_2 activation and the chelating groups of iron species preventing iron leaching.

Based on above-mentioned results, a schematic illustration of photocatalysis promoted heterogeneous Fenton process under visible light irradiation on the α-FeOOH/MesoC composite was proposed in Figure 6. Under visible light irradiation, the α-FeOOH/MesoC composite was excited to generate e^-/h^+ pairs. The e^- plays important roles through two path ways. (1) MesoC≡Fe(III) was reduced to MesoC≡Fe(II) via MesoC (route 1, Figure 6). The reduction of MesoC≡Fe(III) to MesoC≡Fe(II) is the rate limiting step, which determines the generating rate of oxidizing species HO• (route 2, Figure 6).[20,45] The strong α-FeOOH/MesoC interactions via C−O−Fe facilitates the electron transfer between α-FeOOH and MesoC support for the redox cycle of MesoC≡Fe(III)/MesoC≡Fe(II) pair which also suppresses the catalysis of H_2O_2 via route 3.[46] (2) H_2O_2 was catalyzed into HO• and OH^- via route 4. The h^+ also reacts with H_2O to produce HO• via route 5. According to the results of Figure 5, the mixture catalyst without α-FeOOH/MesoC interactions showed low activity implying the minor roles of route 4 and 5. The α-FeOOH/MesoC composite with small crystal size provides more active MesoC≡Fe(III) at the interface between α-FeOOH and MesoC.[47] Accordingly, the photocatalysis enhanced the heterogeneous Fenton process of α-FeOOH/MesoC leading to the higher catalytic activities and mineralization efficiency.

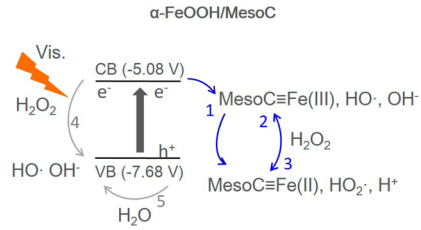

Figure 6. Schematic illustration of photocatalysis promoted heterogeneous Fenton process under visible light irradiation on the α-FeOOH/MesoC composite.

In summary, a novel α-FeOOH/MesoC composite was prepared by incorporating the α-FeOOH mineral with mesoporous carbon via in situ crystallization of adsorbed ferric ions within carboxylic group functionalized mesoporous

DOI: 10.1021/acs.est.6b06429
Environ. Sci. Technol. 2017, 51, 3993−4000

carbon. The α-FeOOH nanocrystals confined in mesoporous frameworks accompanying with surface attached large α-FeOOH microcrystals have catalyst−support interaction via C−O−Fe bond which not only facilitates the high mineralization efficiency of phenol at near neutral conditions and also suppresses the iron leaching. The reused α-FeOOH/MesoC composite showed much higher activity for phenol oxidation and mineralization owing to the interfacial activation of MesoC after heterogeneous Fenton-like process. Visible light irradiation greatly enhances the production of hydroxyl radicals and thus improves the degradation of phenol owing to the increased separation efficiency of photogenerated charges in the presence of H_2O_2. The photogenerated charges then boost the reduction of H_2O_2 to HO• and also the redox cycle of ≡Fe(III)/≡Fe(II) pair. In all, our study will push forward the application of iron and carbon based heterogeneous Fenton-like catalysts for solar energy assisted water treatment and environmental remediation.

■ ASSOCIATED CONTENT

Supporting Information

The Supporting Information is available free of charge on the ACS Publications website at DOI: 10.1021/acs.est.6b06429.

Figure S1−S13 and Table S1: the spectrogram of visible light, FT-IR spectra of MesoC supports, the photographs of MesoC, the mixture and α-FeOOH/MesoC composite, N_2 sorption, phenol oxidation efficiency, the effect of H_2O_2 dosage in dark, the mineralization efficiency of $FeSO_4/H_2O_2$, high resolution XPS spectrum curve fits of C 1s, wide-angle XRD pattern of the reused catalyst, FTIR spectra of the composites before and after reaction, adsorption capacities of phenol, photocatalytic mineralization efficiency of pure α-FeOOH, time profile of temperature variation within 2 h reaction (PDF)

■ AUTHOR INFORMATION

Corresponding Author

*Phone: +86-21-54745704; e-mail: yixin.zhao@sjtu.edu.cn.

ORCID

Yixin Zhao: 0000-0002-8663-9993

Notes

The authors declare no competing financial interest.

■ ACKNOWLEDGMENTS

This work is supported by National Natural Science Foundation of China (21507083) and Shanghai Government (15PJ1404000).

■ REFERENCES

(1) Hartmann, M.; Kullmann, S.; Keller, H. Wastewater treatment with heterogeneous Fenton-type catalysts based on porous materials. *J. Mater. Chem.* **2010**, *20*, 9002−9017.

(2) Zhang, G. Q.; Wang, S.; Yang, F. L. Efficient Adsorption and Combined Heterogeneous/Homogeneous Fenton Oxidation of Amaranth Using Supported Nano-FeOOH As Cathodic Catalysts. *J. Phys. Chem. C* **2012**, *116*, 3623−3634.

(3) Dhakshinamoorthy, A.; Navalon, S.; Alvaro, M.; Garcia, H. Metal Nanoparticles as Heterogeneous Fenton Catalysts. *ChemSusChem* **2012**, *5*, 46−64.

(4) Kan, E.; Huling, S. G. Effects of Temperature and Acidic Pre-Treatment on Fenton-Driven Oxidation of MTBE-Spent Granular Activated Carbon. *Environ. Sci. Technol.* **2009**, *43*, 1493−1499.

(5) Navalon, S.; Alvaro, M.; Garcia, H. Heterogeneous Fenton catalysts based on clays, silicas and zeolites. *Appl. Catal., B* **2010**, *99*, 1−26.

(6) Navalon, S.; Dhakshinamoorthy, A.; Alvaro, M.; Garcia, H. Heterogeneous Fenton Catalysts Based on Activated Carbon and Related Materials. *ChemSusChem* **2011**, *4*, 1712−1730.

(7) Zhou, L. C.; Shao, Y. M.; Liu, J. R.; Ye, Z. F.; Zhang, H.; Ma, J. J.; Jia, Y.; Gao, W. J.; Li, Y. F. Preparation and Characterization of Magnetic Porous Carbon Microspheres for Removal of Methylene Blue by a Heterogeneous Fenton Reaction. *ACS Appl. Mater. Interfaces* **2014**, *6*, 7275−7285.

(8) Qian, X. F.; Fuku, K.; Kuwahara, Y.; Kamegawa, T.; Mori, K.; Yamashita, H. Design and Functionalization of Photocatalytic Systems within Mesoporous Silica. *ChemSusChem* **2014**, *7*, 1528−1536.

(9) Wang, Y. J.; Shi, R.; Lin, J.; Zhu, Y. F. Significant photocatalytic enhancement in methylene blue degradation of TiO_2 photocatalysts via graphene-like carbon in situ hybridization. *Appl. Catal., B* **2010**, *100*, 179−183.

(10) Ribeiro, R. S.; Silva, A. M. T.; Figueiredo, J. L.; Faria, J. L.; Gomes, H. T. Catalytic wet peroxide oxidation: a route towards the application of hybrid magnetic carbon nanocomposites for the degradation of organic pollutants. A review. *Appl. Catal., B* **2016**, *187*, 428−460.

(11) Gu, L.; Zhu, N. W.; Guo, H. Q.; Huang, S. Q.; Lou, Z. Y.; Yuan, H. P. Adsorption and Fenton-like degradation of naphthalene dye intermediate on sewage sludge derived porous carbon. *J. Hazard. Mater.* **2013**, *246*, 145−153.

(12) Ma, W. P.; Kugler, E. L.; Dadyburjor, D. B. Effect of Properties of Various Activated-Carbon Supports and Supported Fe-Mo-Cu-K Catalysts on Metal Precursor Distribution, Metal Reduction, and Fischer−Tropsch Synthesis. *Energy Fuels* **2010**, *24*, 4099−4110.

(13) Hunsom, M.; Autthanit, C. Adsorptive purification of crude glycerol by sewage sludge-derived activated carbon prepared by chemical activation with H_3PO_4, K_2CO_3 and KOH. *Chem. Eng. J.* **2013**, *229*, 334−343.

(14) Adibfar, M.; Kaghazchi, T.; Asasian, N.; Soleimani, M. Conversion of Poly (Ethylene Terephthalate) Waste into Activated Carbon: Chemical Activation and Characterization. *Chem. Eng. Technol.* **2014**, *37*, 979−986.

(15) Guimaraes, I. R.; Oliveira, L. C. A.; Queiroz, P. F.; Ramalho, T. C.; Pereira, M.; Fabris, J. D.; Ardisson, J. D. Modified goethites as catalyst for oxidation of quinoline: Evidence of heterogeneous Fenton process. *Appl. Catal., A* **2008**, *347*, 89−93.

(16) Wang, S.; Zhao, Q. F.; Wei, H. M.; Wang, J. Q.; Cho, M. Y.; Cho, H. S.; Terasaki, O.; Wan, Y. Aggregation-Free Gold Nanoparticles in Ordered Mesoporous Carbons: Toward Highly Active and Stable Heterogeneous Catalysts. *J. Am. Chem. Soc.* **2013**, *135*, 11849−11860.

(17) Wan, Y.; Qian, X. F.; Jia, N. Q.; Wang, Z. Y.; Li, H. X.; Zhao, D. Y. Direct triblock-copolymer-templating synthesis of highly ordered fluorinated mesoporous carbon. *Chem. Mater.* **2008**, *20*, 1012−1018.

(18) Qian, X. F.; Lv, Y. Y.; Li, W.; Xia, Y. Y.; Zhao, D. Y. Multiwall carbon nanotube@mesoporous carbon with core-shell configuration: a well-designed composite-structure toward electrochemical capacitor application. *J. Mater. Chem.* **2011**, *21*, 13025−13031.

(19) Zhu, T.; Ong, W. L.; Zhu, L. L.; Ho, G. W. TiO_2 Fibers Supported beta-FeOOH Nanostructures as Efficient Visible Light Photocatalyst and Room Temperature Sensor. *Sci. Rep.* **2015**, *5*, 1−15.

(20) Ortega-Liebana, M. C.; Hueso, J. L.; Larrea, A.; Sebastiana, V.; Santamaria, J. Feroxyhyte nanoflakes coupled to up-converting carbon nanodots: a highly active, magnetically recoverable, Fenton-like photocatalyst in the visible-NIR range. *Chem. Commun.* **2015**, *51*, 16625−16628.

(21) Hou, X. J.; Huang, X. P.; Ai, Z. H.; Zhao, J. C.; Zhang, L. Z. Ascorbic acid/Fe@Fe_2O_3: A highly efficient combined Fenton reagent to remove organic contaminants. *J. Hazard. Mater.* **2016**, *210*, 170−178.

(22) Song, W. J.; Cheng, M. M.; Ma, J. H.; Ma, W. H.; Chen, C. C.; Zhao, J. C. Decomposition of hydrogen peroxide driven by

DOI: 10.1021/acs.est.6b06429
Environ. Sci. Technol. 2017, 51, 3993−4000

photochemical cycling of iron species in clay. *Environ. Sci. Technol.* **2006**, *40*, 4782−4787.
(23) Zhao, Y. P.; Hu, J. Y.; Jin, W. Transformation of oxidation products and reduction of estrogenic activity of 17 beta-estradiol by a heterogeneous photo-Fenton reaction. *Environ. Sci. Technol.* **2008**, *42*, 5277−5284.
(24) Yu, L.; Wang, C. P.; Ren, X. H.; Sun, H. W. Catalytic oxidative degradation of bisphenol A using an ultrasonic-assisted tourmaline-based system: Influence factors and mechanism study. *Chem. Eng. J.* **2014**, *252*, 346−354.
(25) Duan, X. G.; Ao, Z. M.; Sun, H. Q.; Indrawirawan, S.; Wang, Y. X.; Kang, J.; Liang, F. L.; Zhu, Z. H.; Wang, S. B. Nitrogen-Doped Graphene for Generation and Evolution of Reactive Radicals by Metal-Free Catalysis. *ACS Appl. Mater. Interfaces* **2015**, *7*, 4169−4178.
(26) Herney-Ramirez, J.; Vicente, M. A.; Madeira, L. M. Heterogeneous photo-Fenton oxidation with pillared clay-based catalysts for wastewater treatment: A review. *Appl. Catal., B* **2010**, *98*, 10−26.
(27) Gonzalez-Olmos, R.; Martin, M. J.; Georgi, A.; Kopinke, F. D.; Oller, I.; Malato, S. Fe-zeolites as heterogeneous catalysts in solar Fenton-like reactions at neutral pH. *Appl. Catal., B* **2012**, *125*, 51−58.
(28) Qian, X. F.; Yue, D. T.; Tian, Z. Y.; Reng, M.; Zhu, Y.; Kan, M.; Zhang, T. Y.; Zhao, Y. X. Carbon quantum dots decorated Bi_2WO_6 nanocomposite with enhanced photocatalytic oxidation activity for VOCs. *Appl. Catal., B* **2016**, *193*, 16−21.
(29) Zhang, C.; Yang, H. C.; Wan, L. S.; Liang, H. Q.; Li, H. Y.; Xu, Z. K. Polydopamine-Coated Porous Substrates as a Platform for Mineralized beta-FeOOH Nanorods with Photocatalysis under Sunlight. *ACS Appl. Mater. Interfaces* **2015**, *7*, 11567−11574.
(30) Zuo, X. J.; Chen, M. D.; Fu, D. F.; Li, H. The formation of alpha-FeOOH onto hydrothermal biochar through H_2O_2 and its photocatalytic disinfection. *Chem. Eng. J.* **2016**, *294*, 202−209.
(31) Liu, R. L.; Shi, Y. F.; Wan, Y.; Meng, Y.; Zhang, F. Q.; Gu, D.; Chen, Z. X.; Tu, B.; Zhao, D. Y. Triconstituent Co-assembly to ordered mesostructured polymer-silica and carbon-silica nanocomposites and large-pore mesoporous carbons with high surface areas. *J. Am. Chem. Soc.* **2006**, *128*, 11652−11662.
(32) Wu, Z. X.; Li, W.; Webley, P. A.; Zhao, D. Y. General and Controllable Synthesis of Novel Mesoporous Magnetic Iron Oxide@ Carbon Encapsulates for Efficient Arsenic Removal. *Adv. Mater.* **2012**, *24*, 485−491.
(33) Yang, X. J.; Xu, X. M.; Xu, J.; Han, Y. F. Iron Oxychloride (FeOCl): An Efficient Fenton-Like Catalyst for Producing Hydroxyl Radicals in Degradation of Organic Contaminants. *J. Am. Chem. Soc.* **2013**, *135*, 16058−16061.
(34) Liu, J. Q.; Zheng, M. B.; Shi, X. Q.; Zeng, H. B.; Xia, H. Amorphous FeOOH Quantum Dots Assembled Mesoporous Film Anchored on Graphene Nanosheets with Superior Electrochemical Performance for Supercapacitors. *Adv. Funct. Mater.* **2016**, *26*, 919−930.
(35) Zhou, J. H.; Sui, Z. J.; Zhu, J.; Li, P.; De, C.; Dai, Y. C.; Yuan, W. K. Characterization of surface oxygen complexes on carbon nanofibers by TPD, XPS and FT-IR. *Carbon* **2007**, *45*, 785−796.
(36) Yamashita, H.; Ohtsuka, Y.; Yoshida, S.; Tomita, A. Local Structures of Metals Dispersed on Coal. 1. Change of Local Structure of Iron Species on Brown Coal during Heat Treatment. *Energy Fuels* **1989**, *3*, 686−692.
(37) Yamashita, H.; Yoshida, S.; Tomita, A. Local Structures of Metals Dispersed on Coal. 2. Ultrafine FeOOH as Active Iron Species for Steam Gasification of Brown Coal. *Energy Fuels* **1991**, *5*, 52−57.
(38) Zubir, N. A.; Yacou, C.; Motuzas, J.; Zhang, X. W.; da Costa, J. C. D. Structural and functional investigation of graphene oxide-Fe_3O_4 nanocomposites for the heterogeneous Fenton-like reaction. *Sci. Rep.* **2014**, *4*, 1−8.
(39) Velasco, L. F.; Maurino, V.; Laurenti, E.; Fonseca, I. M.; Lima, J. C.; Ania, C. O. Photoinduced reactions occurring on activated carbons. A combined photooxidation and ESR study. *Appl. Catal., A* **2013**, *452*, 1−8.
(40) Navalon, S.; Dhakshinamoorthy, A.; Alvaro, M.; Garcia, H. Carbocatalysis by Graphene-Based Materials. *Chem. Rev.* **2014**, *114*, 6179−6212.
(41) Zhou, F. Y.; Lu, C.; Yao, Y. Y.; Sun, L. J.; Gong, F.; Li, D. W.; Pei, K. M.; Lu, W. Y.; Chen, W. X. Activated carbon fibers as an effective metal-free catalyst for peracetic acid activation: Implications for the removal of organic pollutants. *Chem. Eng. J.* **2015**, *281*, 953−960.
(42) Wang, X. B.; Qin, Y. L.; Zhu, L. H.; Tang, H. Q. Nitrogen-Doped Reduced Graphene Oxide as a Bifunctional Material for Removing Bisphenols: Synergistic Effect between Adsorption and Catalysis. *Environ. Sci. Technol.* **2015**, *49*, 6855−6864.
(43) Duan, X. G.; Ao, Z. M.; Zhou, L.; Sun, H. Q.; Wang, G. X.; Wang, S. B. Occurrence of radical and nonradical pathways from carbon catalysts for aqueous and nonaqueous catalytic oxidation. *Appl. Catal., B* **2016**, *188*, 98−105.
(44) Liu, R. L.; Shi, Y. F.; Wan, Y.; Meng, Y.; Zhang, F. Q.; Gu, D.; Chen, Z. X.; Tu, B.; Zhao, D. Y. Triconstituent Co-assembly to Ordered Mesostructured Polymer-Silica and Carbon-Silica Nanocomposites and Large-Pore Mesoporous Carbons with High Surface Areas. *J. Am. Chem. Soc.* **2006**, *128*, 11652−11662.
(45) Wang, L.; Cao, M. H.; Ai, Z. H.; Zhang, L. Z. Dramatically Enhanced Aerobic Atrazine Degradation with Fe@Fe_2O_3 Core-Shell Nanowires by Tetrapolyphosphate. *Environ. Sci. Technol.* **2014**, *48*, 3354−3362.
(46) Chou, S. S.; Huang, C. P.; Huang, Y. H. Heterogeneous and homogeneous catalytic oxidation by supported gamma-FeOOH in a fluidized bed reactor: Kinetic approach. *Environ. Sci. Technol.* **2001**, *35*, 1247−1251.
(47) Park, H.; Lee, Y. C.; Choi, B. G.; Choi, Y. S.; Yang, J. W.; Hong, W. H. Energy Transfer in Ionic-Liquid-Functionalized Inorganic Nanorods for Highly Efficient Photocatalytic Applications. *Small* **2010**, *6*, 290−295.

DOI: 10.1021/acs.est.6b06429
Environ. Sci. Technol. 2017, 51, 3993−4000